Int. J. Electrochem. Sci., 12 **(2017)** 1690 – 1699, doi: 10.20964/2017.03.49

International Journal of ELECTROCHEMICAL SCIENCE
www.electrochemsci.org

Short Communication

Electrodeposition of Silver Dendritic-Graphene Composite Film for Photocatalytic Application

Jiliang Xie[1,2,*], *Yanxia Zeng*[2], *Xujie Yang*[1] *and Xingyou Xu*[1,3]

[1] Chemical Engineering Institute, Nanjing University of Science and Technology Nanjing, 210094, P.R. China
[2] Jiangsu Marine Resources Development Research Institute, Lianyungang 222001, P.R. China
[3] School of Chemical Engineering, Huaihai Institute of Technology, Lianyungang 222005, P.R. China
[*]E-mail: jiliangxie_nust3@foxmail.com

Received: 5 December 2016 / *Accepted:* 18 January 2017 / *Published:* 12 February 2017

In this work, a facile one-step electro-deposition approach was reported to synthesize the silver dendritic structure through the multi-walled carbon nanotube (MWCNT) dispersed in AgNO3 solution which was modified with graphene oxide (GO). Scanning electron microscopy was conducted, which demonstrated that the as-synthesized silver material exhibited a well-defined dendritic structure. Besides, according to XRD measurements, the silver was found to be in the cubic phase. GO was demonstrated to be present in silver dendrites through UV-Vis spectroscopy, where GO was electrochemically reduced during the process of silver-deposition. However, based on the preliminary performance test, the pure Ag exhibited a remarkably poor photocatalytic activity, whereas a considerable photocatalytic capacity was observed with the hydrids.

Keywords: One-step electro-deposition; Silver dendrites; Graphene oxide;Photocatalysis; Multi-walled carbon nanotube

1. INTRODUCTION

To process the waste caused by the domestic, agricultural and industrial behaviours becomes a significant challenge in this century. Due to the abundant sunlight resource as well as low carbon emission, artificial photocatalytic systems are of great desirability. For the removal of the dye pollutants, diverse ultraviolet light catalysts have been reported [1, 2]. Nevertheless, compared with the visible light (around 50%) in the natural light, the amount of ultraviolet light (approximate 3%) is considerably low. Hence, for the practical applications, visible-light catalyst becomes remarkably suitable [1, 3-7]. The photocatalyst of plasmon-induced Ag@AgX (X=Cl, Br and I) has been prepared

through the ion exchange or the direct precipitation in prior to reduction [8, 9]. However, owing to the low efficiency of electron transport, the application of these photocatalysts has been restricted.

Graphene, which is a two-dimensional material, has attracted extensive attention because of its outstanding thermal and electrical properties, high surface area and enhanced charge carrier mobility. Graphene oxide (GO), which consists of nearly flat rigidity of carbon atoms where the oxygen-based groups are covalently bonded, has been considered as the precursor of graphene [10]. Besides, GO also exhibits a high surface area, which could be applied to modify metal nanoparticles such as silver, where the Ag nanoparticles could be prepared through various approaches such chemical or photo reduction, atom beam sputtering method, electrochemical technique and the radiation-assisted approach [11]. The in-situ synthesis of Ag NPs assisted by gamma radiation has been recognized as a clean, facial and effective approach [12]. Recently, the reduction of GO through UV, microwave and gamma radiation [13-17]. The nanocomposites of Ag and reduced graphene oxide could be prepared through various approach. Hsu and Chen [18] have reported the synthesis of Ag NPs with a size of 10.3 ± 4.6, 21.4 ± 10.5) and 41.1 ± 12.6 nm via varying the cycle number of microwave irradiation and the deposition of the obtained Ag NPs on RGO, which exhibited an increased surface enhanced Raman scattering (SERS) towards 4-aminothiophenol. Li and Hai [19] have reported the modification of RGO by Ag NPs with a size of 5-10 nm was performed with ethanol through the rapid microwave-assisted approach, which exhibited an improved photocatalytic degradation of Rhodamine B.

Ag nanomaterials, which exhibit fractal and dendritic structures, have received remarkable interest among diverse Ag nanostructures, because of their distinct catalytic, electrical and optical capacities [20, 21]. For instance, silver dendrites have been demonstrated to exhibit various promising applications including catalysis [22], biochemical sensor [23, 24], surface-enhanced Raman scattering (SERS) detection [25]and superhydrophobic surface [26]. Besides, such materials have been synthesized through numerous approaches such as photo reduction [27], elecro-deposition [20, 28], templateless direct growth [29], template technique [30], microwave approach [31] and sono-electrochemical process [32]. In particular, electro-deposition exhibits an advantage of better control the kinetics of reduction and growth among these approaches. In general, this approach is related to the manipulation of the potential of the electrode, where Ag could be reduced under the conditions far from the thermodynamic equilibrium [33]. Moreover, varying the reaction time, the addition of a proper surfactant, the concentration of Ag ion and the employed potential could tune the morphology of the Ag nanostructures [34-36]. Nevertheless, the careful control of the parameters for electro-deposition still is required to produce the desired nanostructures. Hence, to prepare well-defined Ag dendrites, the combination of electro-deposition with the template technique is promising, because a non-equilibrium condition could be provided by the electro-deposition while the morphology of the hierarchical crystallization could be tuned by the template.

Herein, a simple one-step electro-deposition approach was employed to prepare Ag dendrites with the mixed solution of GO-covered MWCNT and AgNO3. GO, which would provide negative sites for nucleating Ag nanoparticles, could facilitate the dispersion of MWCNT in water. In this work, we thoroughly studied the experimental conditions including the composition of the solution as well as the parameters of the electro-deposition to form Ag dendrites. Besides, according to the obtained results, we also proposed an appropriate mechanism. The photodegradation of Rhodamine B (RhB)

indicated that the as-synthesized composites with this approach exhibited a promising capacity towards the environmental purification.

2. EXPERIMENTS

2.1. Chemicals

Graphene oxide powder was commercially available in JCNANO, INC. (China). Multi-walled carbon nanotubes (95%) with a diameter of 40-60 nm as well as a length of 1-2 mm were bought in Shenzhen Nanotech Port Co. Ltd. (China). 3-hydroxytyramine hydrochloride (DA), L-Ascorbic acid (AA, 99%), poly (sodium 4-styrene-sulfonate) (PSS, Mw = 70000), silver nitrate (AgNO3) and Uric acid (UA, 99%) were purchased in Sigma-Aldrich. All the other chemicals were analytically pure and used as received. ITO covered glasses with a R_{est} of 10 ± 2 Ω were bought in Delta Technologies (USA). Besides, the buffer solution (PBS) was produced through mixing KH2PO4 and K2HPO4 solution and adjusting to a proper pH. Noted that all the experiments employed the Milli-Q water (18.2 MΩcm).

2.2. Electrodeposition of silver nanostructures

GO (4 mg) was dispersed into water (10 ml) under ultrasonic for 1 h. Subsequently, MWCNT (2.5 mg) was then added into the obtained dispersion, which was sonicated for 3h to form a homogeneous black suspension. The as-prepared MWCNT covered with GO dispersion could stay stable for several months, where no significant precipitation was observed. To prepare the electro-deposition solutions, the AgNO3 solution (50 mM) prepared freshly was mixed with the MWCNT-GO dispersion at different ratios. Ag was electro-deposited on the ITO electrodes through cyclic voltammetry (CHI430A, CH Instruments, Ausin, TX, USA) combined with a three-electrode system. In this work, a platinum wire and Ag/AgCl with KCl (3M) were utilized as the auxiliary electrode and reference electrode, respectively. The cyclic voltammetry scan was carried out in the range of 0 to -1.6 V, where the scan rate was 20 mV/s. After that, Milli-Q water was used to rinse the ITO for twice. The obtained Ag materials were defined as MWCNT-GO/Ag-1, MWCNT-GO/Ag-2 and MWCNT-GO/Ag-3, while the volume ratios of MWCNT-GO to AgNO3 were 12:1 (3.8 mM $AgNO_3$), 8:1 (5.5 mM $AgNO_3$) and 4:1 (10 mM $AgNO_3$), respectively. The silver specimens of GO/Ag and MWCNT/Ag were also produced with the solutions of GO and $AgNO_3$ as well as MWCNT modified PSS (MWCNT-PSS) and $AgNO_3$ both in a volume ratio of 12:1 as references, where the preparation of MWCNT-PSS was previously reported [21].

2.3. Characterization

The field emission scanning electron microscopy (FeSEM, ZEISS SUPRA 40VP, Germany) as well as the X-ray diffractometer (D8-Advance XRD, Bruker, Germany) combined with Cu K□ radiation was employed to characterize the morphology and the structure of the as-prepared samples,

respectively. The UV-Vis spectrophotometer (Halo RB-10, Dynamic Pty Ltd, AU) was used to conduct the optical measurements with a wavelength ranging from 190 to 800 nm. Besides, Raman Microprobe (Renishaw RM1000) was utilized to perform Raman spectroscopy with a laser light of 514 nm at room temperature.

2.4. Photodegradation of Rhodamine B

The degradation of RhB was used to evaluate the catalytic activity of the nanocomposite of Ag and MWCNT-GO with the visible light. The film, which was deposited on the electrode, was suspended into 50 mL solution of RhB (4 mg/L), where the obtained suspension was placed firstly in dark for 30 min so that the surface of the catalyst was saturated with RhB. Subsequently, the suspension was exposed to a mercury lamp with a high voltage of 250 W for various spans in the range of 0 to 60 min with a interval of 10 min. Thereafter, the catalyst was centrifuged and UV-Vis spectrometer (Optizen POP) was employed to measure the adsorption of the solution specimens at a maximum wavelength (λ_{max}) of 552 nm.

3. RESULTS AND DISCUSSION

Cyclic voltammetry, which is a useful method, was employed to fabricate an electro-deposition device. The first cyclic voltammetric scanning of the ITO electrode in the solution involving the dispersion of MWCNT-PSS/ $AgNO_3$ (curve a), GO/$AgNO_3$ (curve b) or MWCNT-GO/$AgNO_3$ (curve c) was illustrated in Figure 1.

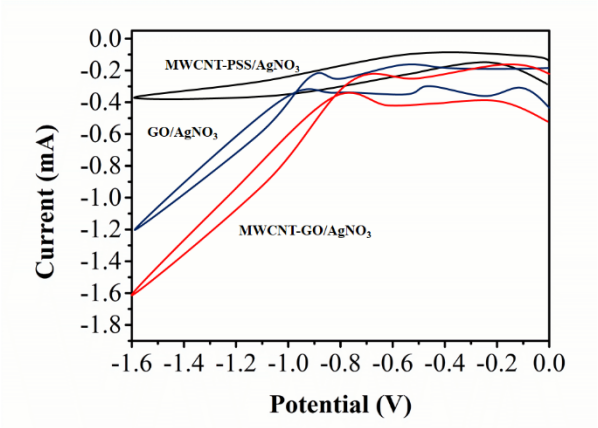

Figure 1. The cyclic voltammograms of the ITO electrodes in the mixed solutions of MWCNT-PSS and $AgNO_3$, GO and $AgNO_3$ as well as MWCNT-GO and $AgNO_3$, respectively.

A tiny reduction peak was observed in the CV profile of MWCNT-PSS/$AgNO_3$ at -0.40 V, which was recognized as the reduction of Ag+ into the metallic Ag [35]. Besides, similar CV profiles were obtained with GO/$AgNO_3$ and MWCNT-GO/$AgNO_3$, where two major reduction peaks were observed. The peak A present at -0.75 V was ascribed to the reduction peak of Ag, which exhibited an

obvious negative shift in comparison to the reduction peak of curve a. This might be caused by the lack of the effective in the solutions of GO/$AgNO_3$ and MWCNT-GO/$AgNO_3$. However, the peak B present in curve b and c might be induced by the non-reversible electrochemical reduction of the hydroxyl, carbonyl and carboxyl groups located at the GO surface [37, 38]. In fact, this peak was not observed in the curve a, which also demonstrated that this process was relevant to GO.

Subsequently, the as-formed Ag with dendritic structure was removed from the electrode and transferred into deionized water. UV-Vis spectroscopy was then carried out to measure the Ag-containing aqueous dispersion, and results were illustrated in Figure 2A. As shown, Curve (a) is the spectrum of MWCNT modified by GO. A sharp peak emerges at 231 nm. It can be ascribed to the $\pi \rightarrow \pi^*$ transition of aromatic C=C bonds in GO [39]. However, for the electro-synthesis of MWCNT/GO/Ag-1, this peak shifts to 257 nm accompanying with the decrease of peak intensity. This indicates that GO in the nanocomposite was reduced [40]. Moreover, a single broad absorption peak at 380 nm which was corresponded to the surface plasmon resonance (SPR) absorption of Ag is clearly observed. This result further confirms the formation of Ag. The peak intensity and peak position of Ag SPR band are highly related to the size and shape of nanocrystals. The asymmetric peak with long tail in the curve reveals that a supermolecular structure may be formed [35]. Raman spectroscopy was also used to further confirm the reduction of GO. As can be seen from Figure 2B, two peaks at 1600 cm^{-1} and 1350 cm^{-1} are observed in the Raman spectra of both GO and GO/Ag. The peak emerges at higher wavenumber can be ascribed to the graphite (G) bands, while the lower one is corresponded to the diamondoid (D) bands. It is worth noting that, the peak intensity ratio of D to G (I_D/I_G) increases from 0.89 to 1.07. This suggests that defect-rich graphite were produced through the reduction process [41].

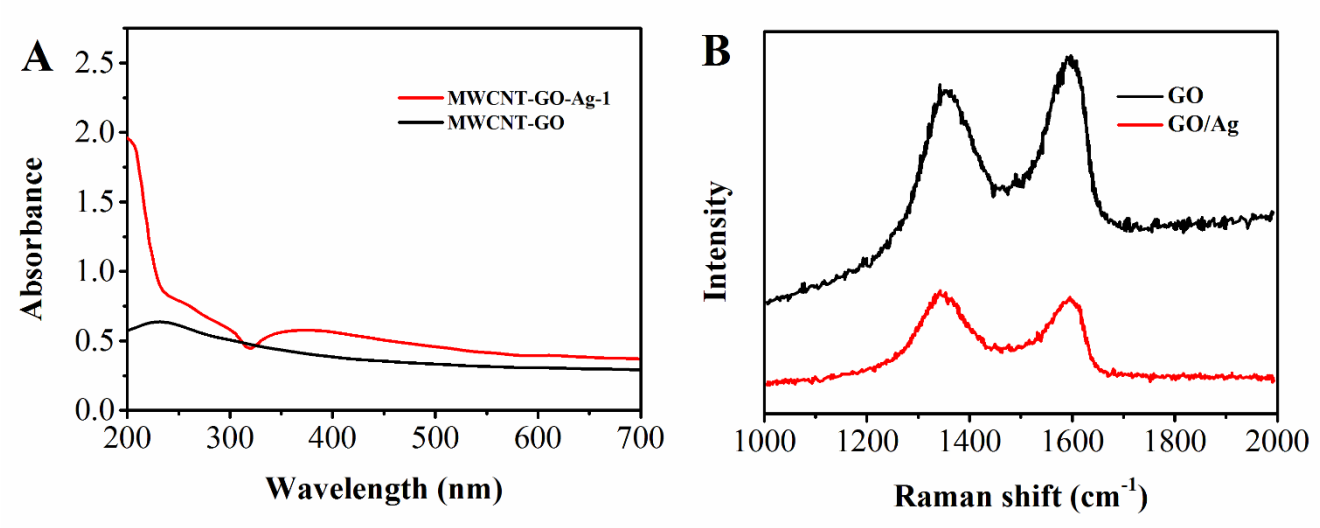

Figure 2. (A) UV-Vis absorption spectra of MWCNT/GO and MWCNT-GO/Ag-1 aqueous dispersion; (B) Raman spectra of GO and GO/Ag.

Structural analysis of MWCNT-GO/Ag with different Ag ratio was measured by XRD, and results were shown in Figure 3. As can be seen from Figure 3A, a characteristic peak corresponding to the pristine GO powder at 11.1° can be clearly observed. It is responded to the (001) plane of GO with

an inter-planar space of 0.82 nm [42]. In contrast, this peak does not emerge in the other XRD patterns of prepared MWCNT-GO/Ag samples. This further demonstrates that a process of GO reduction was happened through the electro-deposition. In addition, the cubic phase of Ag (JCPDS file No. 04-0783) can also be observed in the XRD patterns of the samples of MWCNT-GO/Ag. The peak with a high intensity at 36.50° is assigned to the (111) plane of Ag cubic phase. This suggests that (111) plane is preferably formed through the Ag deposition process under the experimental conditions. With the rise of Ag proportion, intensity of these peaks at 42.67°, 62.92°, 75.90° and 79.83°gradually increase. Those peaks are related to the (200), (220), (311) and (222) plane of Ag fcc (face-centered-cube) crystal, respectively.

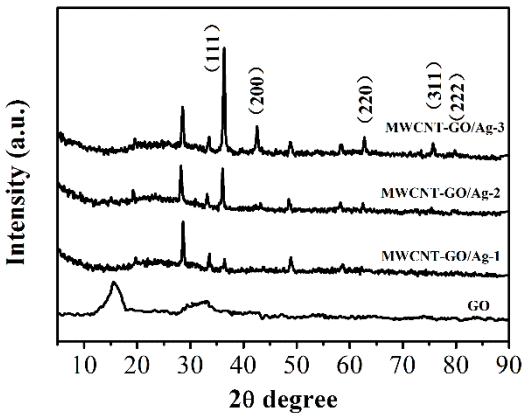

Figure 3. XRD patterns of MWCNT-GO/Ag with different Ag proportion: GO powder, MWCNT-GO/Ag-1, MWCNT-GO/Ag-2 and MWCNT-GO/Ag-3 coated ITO.

MWCNT-GO/Ag samples were prepared using electro-deposition in a solution containing MWCNT, GO and $AgNO_3$. Surface morphology of prepared MWCNT-GO/Ag samples were performed by SEM, and images of were listed in Figure 4. As shown, spherical-shaped Ag with an average diameter of 50 nm were observed in Figure 4A, while no dendrite structure was constructed (Inset of Figure 4A). In Figure 4B, two different types of Ag are observed in the sample of MWCNT-PSS/$AgNO_3$. One is Ag with spherical structure, and the other is Ag with dendrite structure which is only in the early formation stage. However, in the specimen of MWCNT-GO/Ag, well-defined Ag with dendritic structure was formed, and the length of central stem is approximately 5 μm. Under the experimental condition, a high negative potential vs. the real reduction potential of Ag can be regarded as the non-equilibrium condition which is available for the formation of dendritic fractals [43]. It is worth noting that, with the absence of MWCNT, dendritic structure did not form indicating that the existence of MWCNT is remarkably important towards the construction of the dendritic structure. This may be caused by the linear structure and negatively charged surface of MWCNT. Normally, MWCNT is electric neutrality. However, negatively charged PSS and GO coat on the MWCNT surface on which positively charged silver ions can be easily trapped and then form nucleation sites for the formation of Ag nanoparticles. The electric field gradient which was formed around the Ag nanoparticles on the MWCNT surface is significantly larger compared with that on the surface of ITO.

Therefore, Ag with a dendritic structure was constructed as a result of this electric field. This fractal growth could be illustrated by a so-called diffusion-limited-aggregation (DLA) model which elucidates the cluster growth from particle adhesion to seed formation on the contact surface after the reduction process [44, 45]. In this study, Ag ions on the surface of ITO are exhausted after the initial reduction process, and thus the potential drops immediately due to the absence of supporting electrolyte. In contrast, with a supporting electrolyte Ag ions can migrate from the solution of bulk to the top of the preformed Ag dendrites as a result of higher electric field gradient [46]. Subsequently, Ag ions combine successively with the preformed Ag nanoparticles to construct the stems of dendrites. Therefore, for the growth procedure of Ag with dendritic structure, the diffusion of Ag ions is of crucial importance [47]. In addition, the size of Ag dendrites in MWCNT-rGO/Ag is much larger than that of MWCNT/Ag, which may be caused by the non-conductive PSS coated on the surface of MWCNT, where the conductivity of MWCNT decreased, and then the formation of Ag dendrites was hindered. However, the existence of GO as well as MWCNT are contributed to the generation of Ag dendrites. In the former case, a number of functional groups on the GO surface are present under electrochemical conditions.

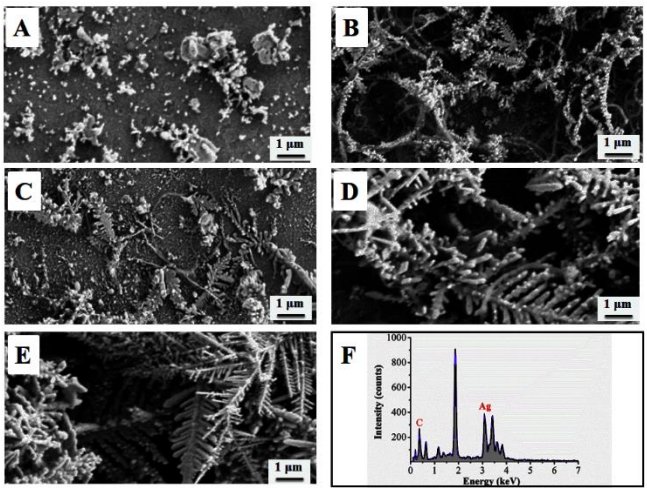

Figure 4. SEM images of electrodepositions of GO/Ag (A). Inset: high magnification; MWCNT-PSS/Ag(B); MWCNT-GO/Ag-1 (C); MWCNT-GO/Ag-2 (D); MWCNT-GO/Ag-3 (E). EDS of MWCNT-GO/Ag-1 (F).

Those groups facilitate the nucleation of Ag particles in the reduction process as the active sites. In the latter case, surface defects of MWCNT like the kinked structure can also serve as nucleation sites. Therefore, adding both GO and MWCNT could accelerate the Ag dendrites formation under the experimental condition. After the process depended on concentration, the multi-branched structure has been prepared [48]. The relationships between the growth rate of Ag dendrites and the concentration of Ag ions were investigated, where various samples with different volume ratios of MWCNT-GO to $AgNO_3$ were measured. As shown in the Figures 4C and 4D, the surface density and coverage of the Ag dendrites both increased with a rise of $AgNO_3$ concentration to 5.5 mM from 3.8

mM. For MWCNT-GO/Ag-2, single Ag particles and Ag dendrites both can be observed on the ITO surface. This suggests that the dendrites have not grown completely. When concentration of Ag was increased further to 10 mM, a large number of well-defined Ag dendrites are formed on the electrode. Owing to those dendrites, the active surface area of electrode was significantly enhanced (Figure 4E). In addition, EDS was also carried out. The results further confirm that the obtained products are primarily consist of metallic Ag, reduced GO and MWCNT.

As-prepared MWCNT-GO/Ag nanocomposites were applied to photodegradation of RhB under visible light irradiation, and RhB concentration as a function of irradiation time was investigated. The results were listed in Figure 5. In order to achieve an equilibrium adsorption state, a dark adsorption procedure was carried out for 30 min before the irradiation of visible light. As shown, the MWCNT-GO/Ag nanocomposite possesses extraordinary catalytic activity for the degradation of RhB which is much higher than that of GO catalyst. Obviously, the photodegradation of RhB over MWCNT-GO/Ag nanocomposite is strongly affected by the microwave cyclic time. This may be related to the reduced GO, since it can effectively promote the transfer of photo-generated electron. However, continuously rising the microwave cyclic time, performance of photodegradation decreases obviously. This can be ascribed to re-oxidation of reduced GO. The catalytic performance of MWCNT-GO/Ag nanocomposite was compared with other catalysts in the literature in Table 1. Results indicate that our proposed MWCNT-GO/Ag nanocomposite is a competitive catalyst with excellent catalytic performance.

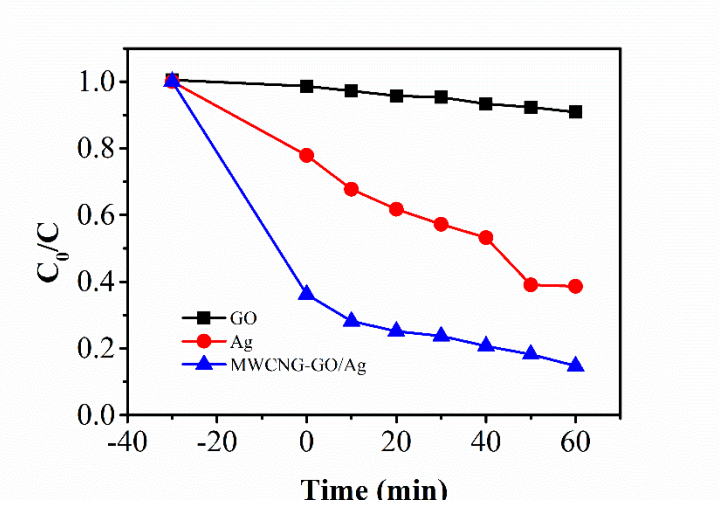

Figure 5. Degradation of RhB over GO, Ag, and MWCNT-GO/Ag nanocomposite under visible light condition. *C* is concentration at time *t*, and *Co* is the RhB concentration in initial solution.

Table 1 Performance comparison of the proposed MWCNT-GO/Ag nanocomposite and other reported catalysts towards the reduction of RhB.

Catalyst	Rate constant (min^{-1})	Reference
Bimetallic Pt–Cu	2.7	[49]
Ag-Fe_3O_4	0.42	[50]
Polydopamine microparticles	0.228	[51]
Sm-doped CeO_2	0.161	[52]
MWCNT-GO/Ag	0.273	This work

4. CONCLUSIONS

In the present work, a one-step electrochemical deposition method for synthesizing Ag with dendritic structure was introduced. During the process of electro-deposition, GO was reduced, which further was confirmed by UV-Vis and Raman spectroscopy. XRD and SEM characterizations show that the as-formed silver is cubic phase with dendritic structure. The presence of MWCNT is of critical importance towards the production of the dendritic structures. As-prepared MWCNT-GO/Ag nanocomposites were applied to photodegradation of RhB under visible light irradiation, and results show that the nanocomposites have considerable photocatalytic activity which is much higher than that of pure Ag.

References

1. Y. Min, K. Zhang, W. Zhao, F. Zheng, Y. Chen and Y. Zhang, *Chem. Eng. J.*, 193 (2012) 203.
2. Y. Gao, X. Pu, D. Zhang, G. Ding, X. Shao and J. Ma, *Carbon*, 50 (2012) 4093.
3. Y. Min, K. Zhang, Y. Chen and Y. Zhang, *Chem. Eng. J.*, 175 (2011) 76.
4. Z. Xiong, L.L. Zhang, J. Ma and X. Zhao, *Chemical Communications*, 46 (2010) 6099.
5. H. Fu, C. Pan, W. Yao and Y. Zhu, *J. Phys. Chem. B.*, 109 (2005) 22432.
6. H. Zhang, X. Fan, X. Quan, S. Chen and H. Yu, *Environmental Science & Technology*, 45 (2011) 5731.
7. J. Zhao, T. Wu, K. Wu, K. Oikawa, H. Hidaka and N. Serpone, *Environmental Science & Technology*, 32 (1998) 2394.
8. P. Wang, B. Huang, X. Qin, X. Zhang, Y. Dai, J. Wei and M.H. Whangbo, *Angewandte Chemie International Edition*, 47 (2008) 7931.
9. H. Xu, J. Yan, Y. Xu, Y. Song, H. Li, J. Xia, C. Huang and H. Wan, *Appl. Ctatl. B-Environ.*, 129 (2013) 182.
10. D. Chen, H. Feng and J. Li, *Chemical Reviews*, 112 (2012) 6027.
11. Q. Tran and A. Le, *Advances in Natural Sciences: Nanoscience and Nanotechnology*, 4 (2013) 033001.
12. C. Jonah and B. Rao, Radiation Chemistry: Present Status and Future Trends, Elsevier 2001.
13. Y. Ding, P. Zhang, Q. Zhuo, H. Ren, Z. Yang and Y. Jiang, *Nanotechnology*, 22 (2011) 215601.
14. Y. Zhang, H. Ma, Q. Zhang, J. Peng, J. Li, M. Zhai and Z. Yu, *Journal of Materials Chemistry*, 22 (2012) 13064.
15. L. Dumée, C. Feng, L. He, Z. Yi, F. She, Z. Peng, W. Gao, C. Banos, J. Davies and C. Huynh, *Carbon*, 70 (2014) 313.
16. Z. Li, W. Zhang, J. Guo, B. Yang and J. Yuan, *Vacuum*, 117 (2015) 35.
17. S. Rella, A. Giuri, C. Corcione, M. Acocella, S. Colella, G. Guerra, A. Listorti, A. Rizzo and C. Malitesta, *Vacuum*, 119 (2015) 159.
18. K. Hsu and D. Chen, *Nanoscale Res Lett*, 9 (2014) 1.
19. Q. Li and P. Hai, *Mat. Sci. Semicon. Proc.*, 22 (2014) 16.
20. S. Wang, L. Xu, Y. Wen, H. Du, S. Wang and X. Zhang, *Nanoscale*, 5 (2013) 4284.
21. L. Fu, T. Tamanna, W. Hu and A. Yu, *Chemical Papers*, 68 (2014) 1283.
22. J. Huang, S. Vongehr, S. Tang, H. Lu, J. Shen and X. Meng, *Langmuir*, 25 (2009) 11890.
23. T. You, O. Niwa, M. Tomita and S. Hirono, *Anal. Chem.*, 75 (2003) 2080.
24. L. Fu, G. Lai, B. Jia and A. Yu, *Electrocatalysis*, 6 (2015) 72.
25. Q. Zhang, Y. Chen, Z. Guo, H. Liu, D. Wang and X. Huang, *ACS Applied Materials & Interfaces*, 5 (2013) 10633.

26. X. Zhang, F. Shi, J. Niu, Y. Jiang and Z. Wang, *Journal of Materials Chemistry*, 18 (2008) 621.
27. Y. Zhou, S. Yu, C. Wang, X. Li, Y. Zhu and Z. Chen, *Adv. Mater.*, 11 (1999) 850.
28. L. Fu, G. Lai, P.J. Mahon, J. Wang, D. Zhu, B. Jia, F. Malherbe and A. Yu, *RSC Advances*, 4 (2014) 39645.
29. W. Ren, S. Guo, S. Dong and E. Wang, *J. Phys. Chem. C.*, 115 (2011) 10315.
30. J. Zhang, F. Huang and Z. Lin, *Nanoscale*, 2 (2010) 18.
31. M. Noroozi, A. Zakaria, M.M. Moksin, Z.A. Wahab and A. Abedini, *International Journal of Molecular Sciences*, 13 (2012) 8086.
32. S. Tang, X. Meng, H. Lu and S. Zhu, *Mater. Chem. Phys.*, 116 (2009) 464.
33. G.M. Oliveira and I.A. Carlos, *Journal of Applied Electrochemistry*, 39 (2009) 1217.
34. S. Tang, X. Meng, H. Lu and S. Zhu, *Mater. Chem. Phys.*, 116 (2009) 464.
35. S. Kaniyankandy, J. Nuwad, C. Thinaharan, G. Dey and C. Pillai, *Nanotechnology*, 18 (2007) 125610.
36. A. Moradi Golsheikh, N. Huang, H. Lim, R. Zakaria and C. Yin, *Carbon*, 62 (2013) 405.
37. M. Raj and S. John, *J. Phys. Chem. C.*, 117 (2013) 4326.
38. Y. Shao, J. Wang, M. Engelhard, C. Wang and Y. Lin, *Journal of Materials Chemistry*, 20 (2010) 743.
39. J. Paredes, S. Villar-Rodil, A. Martínez-Alonso and JD. Tascón, *Langmuir*, 24 (2008) 10560.
40. Y. Zhou, Q. Bao, L. Tang, Y. Zhong and K. Loh, *Chemistry of Materials*, 21 (2009) 2950.
41. J. Yang, J. Zheng, H. Zhai and L. Yang, *Cryst Res Technol*, 44 (2009) 87.
42. T. Nakajima, A. Mabuchi and R. Hagiwara, *Carbon*, 26 (1988) 357.
43. X. Meng, S. Tang and S. Vongehr, *Journal of Materials Science & Technology*, 26 (2010) 487.
44. T. Witten and L. Sander, *Physical Review Letters*, 47 (1981) 1400.
45. E. Ben-Jacob and P. Garik, *Nature*, 343 (1990) 523.
46. N. Abbasi, P. Shahbazi and A. Kiani, *Journal of Materials Chemistry A*, 1 (2013) 9966.
47. H. Xun, G.Z. Wang, Y. Wang, W. Zhu and X. Shen, *Chinese Journal of Chemical Physics*, 23 (2010) 596.
48. P. Zhou, Z. Dai, M. Fang, X. Huang, J. Bao and J. Gong, *J. Phys. Chem. C.*, 111 (2007) 12609.
49. H. Singh, N. Gupta, S. Sharma and R. Sharma, *Colloids and Surfaces A: Physicochemical and Engineering Aspects*, 416 (2013) 43.
50. L. Ai, C. Zeng and Q. Wang, *Catalysis Communications*, 14 (2011) 68.
51. S. Du, Z. Liao, Z. Qin, F. Zuo and X. Li, *Catalysis Communications*, 72 (2015) 86.
52. S. Kundu, N. Sutradhar, R. Thangamuthu, B. Subramanian, A. Panda and M. Jayachandran, *Journal of Nanoparticle Research*, 14 (2012) 1.